ChemPubSoc Europe

DOI: 10.1002/cctc.201500041

CHEMCATCHEM Full Papers

Iron(II) Disulfides as Precursors of Highly Selective Catalysts for Hydrodeoxygenation of Dibenzyl Ether into Toluene

Na Ji, Xingyu Wang, Claudia Weidenthaler, Bernd Spliethoff, and Roberto Rinaldi*[a]

In this report, we show that nanocrystalline pyrite and marcasite (FeS_2), supported on SBA-15, aerosil SiO_2, activated carbon or Al_2O_3, are precursors of highly active catalysts for the hydrodeoxygenation of dibenzyl ether into toluene. High yields of toluene (up to 100%) were achieved in experiments performed at 250 °C under initial H_2 pressure of 100 bar for 2 h. In the recycling experiments, results from XRD and XPS analyses indicate that a fresh surface, formed upon the chemical transformation of FeS_2 into $Fe_{(1-x)}S$, is responsible for the high activity and high selectivity achieved in the conversion of dibenzyl ether into toluene.

Introduction

Iron(II) disulfides (i.e. pyrite or marcasite) are well known to enhance the reactivity of coals towards liquefaction under elevated H_2 pressure (100–300 bar) at high temperatures (350–450 °C).[1,2] In addition, there are also a few reports to suggest that sulfided iron catalysts facilitate the liquefaction of technical lignins under high severity conditions.[3–6] Analyzing the key studies published over the last 50 years, one can easily identify two main classes of Fe–S catalysts that have been explored for coal and lignin liquefaction. The first class comprises bulk iron(II) disulfides of low surface area ($<2\,m^2g^{-1}$), which have been almost exclusively applied to direct coal liquefaction.[1,2,6] The second class encompasses sulfided iron species formed in situ by reactions of an iron compound [e.g. ferrocene, $Fe(NO_3)_3$] and a sulfur source (e.g. CS_2, S_8). These Fe–S materials were explored for lignin liquefaction.[4,5] Owing to the low surface area of bulk iron(II) disulfides, and the undefined chemical nature of sulfided iron catalysts formed in situ, the factors accounting for the catalytic activity of both classes of Fe–S materials remain unclear. Surprisingly, despite evidence demonstrating the potential of these materials for liquefaction of lignin and coal, the relationships between structure and catalysis of (bulk) iron(II) disulfides have been attracted little attention. Indeed, most knowledge in this field originates from reports dated back to the 1980s.[2,7,8] More recently, some in-depth computational studies of pyrite surface and structure were reported.[9–15] From a catalysis perspective, therefore, revisiting this research field with modern techniques for preparation and characterization of highly dispersed iron(II) disulfide phases on supports exhibiting high surface area could contribute insights as to whether these materials can be useful as catalysts or catalyst precursors in the conversion of biomass-derived aromatic streams.

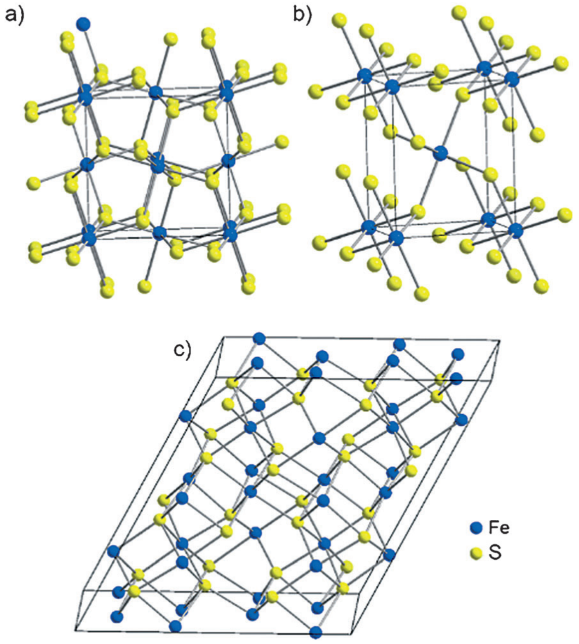

Figure 1. Sketch of the crystalline structure of a) pyrite, b) marcasite, and c) pyrrhotite (based on the NiAs unit cell).

Pyrite is a polymorph of iron(II) disulfide (Figure 1 a) crystallized in a cubic crystal structure.[16] It comprises discrete S_2^{2-} units with an S–S distance (2.195 Å) similar to that expected for an S–S single bond (2.00 to 2.11 Å).[16,17] Thus, pyrite is properly described as $Fe^{2+}S_2^{2-}$.[17,18] Marcasite is another polymorph of iron(II) disulfide with an orthorhombic crystal structure (Figure 1 b).[16,17] Under H_2 pressure at temperatures above 200 °C, pyrite releases H_2S and converts into a class of non-stoi-

---

[a] Dr. N. Ji, X. Wang, Dr. C. Weidenthaler, B. Spliethoff, Dr. R. Rinaldi
Max-Planck-Institut für Kohlenforschung
Kaiser-Wilhelm-Platz 1, Mülheim an der Ruhr (Germany)
Fax: (+49) 208-306-2995
E-mail: rinaldi@kofo.mpg.de

chiometric iron(II) sulfides, called pyrrhotites ($Fe_{(1-x)}S$ where $0 \leq x \leq 0.125$).[2,8]

Pyrrhotites possess a NiAs-type structure (Figure 1 c), which can exhibit monoclinic or hexagonal crystal symmetry.[17,19,20] One can describe the monoclinic pyrrhotite by subtracting one-eighth iron atoms from the hexagonal FeS structure, so that the resulting structure contains alternating layers of full Fe sites and layers of Fe sites with vacancies.[19,20] The monoclinic structure can be converted to hexagonal at temperatures above 300 °C. The fast diffusion of Fe^{II} vacancies at these temperatures creates a random vacancy distribution.[19,20] As a result, the phase transition is reversible. However, at temperatures lower than 300 °C, the diffusion of vacancies is inhibited, thereby, metastable hexagonal pyrrhotite structures can be locked by a quenching process.[28] Troilite, the iron-rich end-member of the pyrrhotites, is an ideal or nearly stoichiometric iron(II) sulfide ($Fe_{(1-x)}S$ where $0 \leq x \leq 0.05$).[19,20] It shows a NiAs derived-structure with hexagonal symmetry, which is stable at room temperature (RT).

The role of each iron(II) sulfide and iron(II) disulfide in the coal or lignin liquefaction processes is only partially understood.[2,7,8] Although pyrrhotite (prepared in advance) shows a lower activity than pyrite in coal liquefaction, pyrrhotite formed in situ was demonstrated to possess 'very good' catalytic activity.[8] Kodaira et al. surmised that the formation of the fresh surface with the chemical change from pyrite to pyrrhotite is the cause of the high activity of pyrite.[8] In turn, Montano et al. demonstrated that troilite shows lowest activity among $Fe_{(1-x)}S$ structures.[2] Moreover, Baldwin and Vinciguerra suggested that H_2S, formed upon the reduction of FeS_2 to $Fe_{(1-x)}S$, could be an active homogeneous catalyst for coal liquefaction.[7]

In this report, we present the synthesis, characterization, and catalytic performance of supported nanocrystalline iron(II) disulfides supported on SBA-15, aerosil SiO_2, activated carbon (AC), or γ-alumina (Al_2O_3). The purpose of this work is to determine whether FeS_2 materials can act as catalysts or catalyst precursors for the hydrodeoxygenation (HDO) of dibenzyl ether into toluene under conditions of lower severity (100 MPa H_2, 250 °C) than those applied for coal or lignin liquefaction (100–350 MPa H_2, 350–450 °C). This report is organized in three sections. First, the synthesis and characterization of the structural features of the supported nanocrystalline FeS_2 materials are presented. Second, the catalytic properties of the materials in the HDO of dibenzyl ether are examined under varying conditions. Third, in the recycling experiments, insight into the Fe–S species involved in the catalysis of HDO of dibenzyl ether is provided by XRD and XPS analyses.

Results and Discussion

Synthesis and Characterization of FeS_2 Materials

To synthesize FeS_2 supported on SBA-15, SiO_2, AC, or Al_2O_3, incipient impregnation of the supports with an iron(III) nitrate solution was performed in order to provide a nominal loading of iron(III) of 10 wt %. The materials were calcined at 400 °C for 2 h in a quartz tube. For the Fe^{III}/AC material, thermal treatment was performed under argon flow. In sequence, the air or argon atmosphere was switched by an H_2S atmosphere. The material was sulfided at 400 °C for an additional 2.5 h. This procedure led to the reduction of Fe^{III} to Fe^{II} as evidenced by the formation of elemental sulfur, which sublimated and deposited as a pale yellow layer on the cold exit of the quartz tube. Importantly, the formation of iron(II) disulfides was also confirmed by X-ray powder diffraction (XRD). XRD patterns in Figure 2 indicate that the sulfidation procedure renders pyrite (major product) and marcasite (minor product) irrespective of the support.

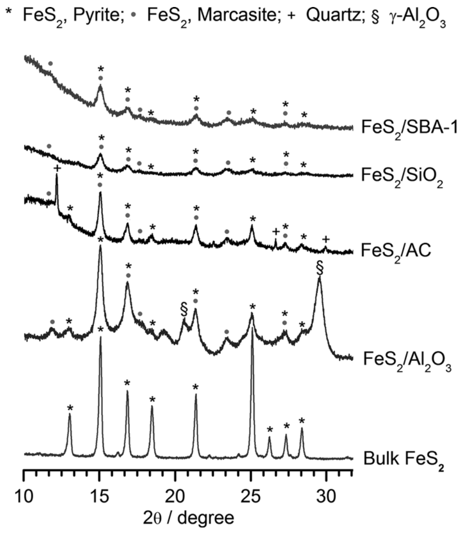

Figure 2. XRD patterns of FeS_2 supported on SBA-15, SiO_2, AC, Al_2O_3, and bulky FeS_2 (pyrite).

In previous studies on liquefaction of coal in the presence of bulk pyrite and other iron(II) sulfides, no information was provided about the material history concerning its handling under air.[2,7,8] Nonetheless, it is known that finely divided iron(II) sulfide powders may oxidize to iron oxides and (thio)sulfates when exposed to humid air.[17,21–23] To verify whether FeS_2/AC is an air-sensitive material, the fresh sulfided material was exposed to air for 24 h. Figure 3 shows that the XRD reflections characteristic to pyrite and marcasite disappeared from the XRD pattern of the FeS_2/AC sample exposed to air. This result demonstrates that the nanocrystalline FeS_2 phases are air-sensitive. As will be presented in the next section, this material also shows a poor catalytic performance, compared with FeS_2/

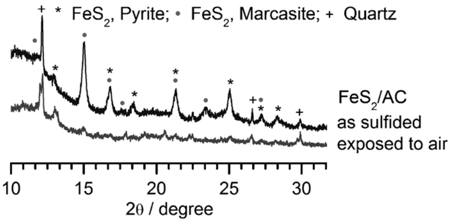

Figure 3. XRD patterns of FeS_2/AC 'as sulfided' and exposed to air for 24 h.

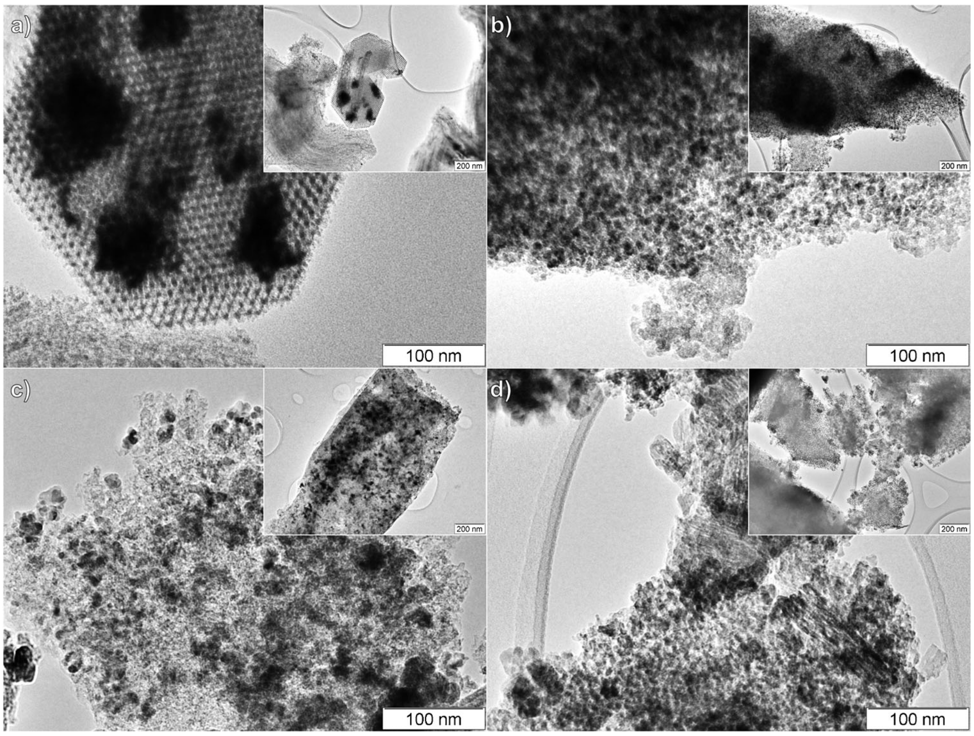

Figure 4. TEM images of a) FeS_2/SBA-15, b) FeS_2/SiO_2, c) FeS_2/AC, and d) FeS_2/Al_2O_3. The insets provide a thumbnail view for representative material particles. Scale bars = 100 nm (inset = 200 nm).

AC handled under argon. Accordingly, material transfer and other procedures described here were performed under argon.

Displayed in Figure 4 are the TEM images of FeS_2/SBA-15, FeS_2/SiO_2, FeS_2/AC, and FeS_2/Al_2O_3. The average size of individual FeS_2 particles is in the range of 5–20 nm for FeS_2/SBA-15, 5–10 nm for FeS_2/SiO_2, 10–20 nm for FeS_2/AC, and 5–35 nm for FeS_2/Al_2O_3. In general, the TEM images show that FeS_2 particles are quite well-dispersed on the supports. However, for FeS_2/SBA-15 (Figure 4 a), it is apparent that FeS_2 is poorly dispersed. Moreover, EDX analyses indicate that the Fe:S atom ratio is nearly 1:2 in FeS_2/SBA-15, FeS_2/SiO_2 and FeS_2/Al_2O_3, but 1:3 in FeS_2/AC. The sulfidation procedure resulted in the formation of S_8. However, AC itself is reported to oxidize H_2S to S_8 at high temperatures.[24,25] A part of the S_8 content stays entrapped in the pore structure of AC, as determined by XPS analysis (Figure 7 c).

Summarized in Table 1 are the textural properties of the sulfided materials and their parent supports. FeS_2/SBA-15 and FeS_2/Al_2O_3 display values of surface area 3 to 11 % smaller than the respective supports. The small decrease in the surface area is in line with the TEM visualization of the FeS_2 particles partially filling the pore system of SBA-15 and Al_2O_3 supports (Figures 4 a and 4 d) in an inhomogeneous manner. This observation is particularly notable for FeS_2/SBA-15 in which only some channels of SBA-15 are loaded with FeS_2 (Figure 4 a). This fact seems to be the reason for no change in the pore volume of SBA-15 materials to be detected by N_2 physisorption analysis. In contrast, FeS_2 particles are better dispersed on AC and SiO_2 (Figures 4 b and 4 c). Hence, FeS_2/AC and FeS_2/SiO_2 have values of surface area, as well as pore volume, about 25 to 35 % smaller than the respective supports.

Catalytic properties of supported FeS_2 materials

To find the conditions of lowest severity needed for the catalytic conversion of dibenzyl ether, experiments (Figure 5) with FeS_2/AC varying a) temperature (150–250 °C), b) initial pressure of H_2 (15–100 bar), and c) reaction time (0–4 h) were performed. Summarized in Figure 5 are the results of the optimization of the reaction parameters in the catalytic conversion of dibenzyl ether with FeS_2/AC suspended in cyclohexane (solvent). Figure 5 shows that full conversion of dibenzyl ether into toluene is achieved at a temperature of 250 °C under a H_2 pressure of 100 bar in 2 h. Accordingly, we chose these conditions to further evaluate the catalytic performance of the other materials.

Table 1. Textural properties of the supports and FeS_2 supported materials.

Entry	Material	S_{BET} [$m^2 g^{-1}$]	Pore volume [$cm^3 g^{-1}$]	Pore diameter [nm]
1	SBA-15	814	0.96	5.2
2	FeS_2/SBA-15	791	0.96	4.1
3	SiO_2	424	0.76	5.3
4	FeS_2/SiO_2	334	0.57	5.3
5	AC	626	0.20	3.7
6	FeS_2/AC	480	0.13	3.5
7	Al_2O_3	122	0.25	6.2
8	FeS_2/Al_2O_3	109	0.17	5.3

Listed in Table 2 are the results obtained from blank experiments and catalyst screening. Regarding the blank experiments, Entry 1 shows that a 1 % conversion of dibenzyl ether was achieved in a blank experiment in absence of catalyst. This result indicates that the substrate is thermally stable at 250 °C. This observation agrees with previous studies on the kinetics of thermolysis of dibenzyl ether, which showed that the reaction takes place at appreciable rates at temperatures higher than 350 °C.[26] However, entry 2 shows that a 29 % conversion of dibenzyl ether into toluene (carbon selectivity, 38 %), benzyl alcohol (23 %) and benzaldehyde (41 %) was reached in a blank experiment conducted in the presence of unloaded AC. The presence of low levels of benzaldehyde seems to be related to the presence of (Brønsted) acid sites in AC, as benzaldehyde is

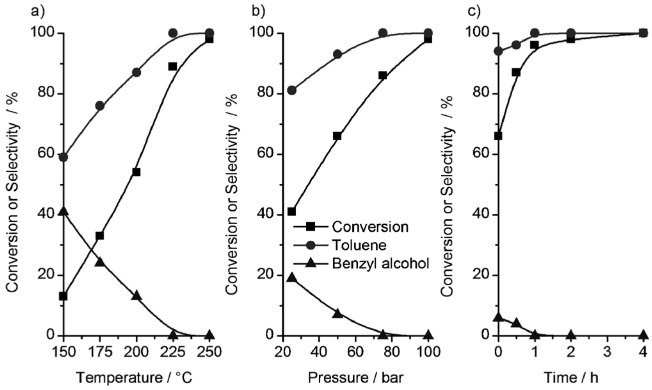

Figure 5. Optimization of the reaction parameters in the conversion of dibenzyl ether in the presence of FeS_2/AC. a) Reaction temperature (initial pressure of H_2: 100 bar, reaction time: 2 h); b) initial pressure of H_2 (reaction temperature: 250 °C; reaction time: 2 h); c) reaction time (initial pressure of H_2: 100 bar, reaction temperature: 250 °C) on the HDO of dibenzyl ether. Cyclohexane was used as solvent. The reaction time was recorded upon reaching the aforementioned temperatures (heating rate 10 °C min^{-1}).

Table 2. Conversion of dibenzyl ether in the absence and presence of different iron catalysts.[a]

Entry	Material	Conv. [%]	Carbon selectivity [%] 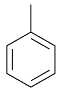	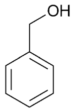	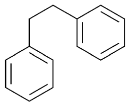	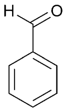
1	None	1	0.7	0.5	0	1.4
2	AC	29	38	23	0	41
3	FeS_2/AC	98	100	0	0	0
4	FeS_2/SBA-15	98	80	0	16	0
5	FeS_2/SiO_2	98	87	0	12	0
6	FeS_2/Al_2O_3	95	98	0	0	0
7	FeS_2/AC-Air	53	70	7	0	23
8	Fe_2O_3/AC	50	78	12	0	10

[a] Reaction conditions: dibenzyl ether (2.5 mmol), *n*-decane (0.7 mmol, internal standard for GC), catalyst (0.15 g) and cyclohexane (15 mL, solvent) under 100 bar H_2 (measured at RT), 250 °C for 2 h.

not a typical product of metal-catalyzed hydrogenolysis of dibenzyl ether,[27–29] but a product of acid-catalyzed cleavage of the ether bond.[30]

Shown in Scheme 1 is a proposed pathway for the formation of benzaldehyde and toluene by acid catalysis ("A" stands for an acid site). The proposed pathway involves the formation of phenylmethylium, upon cleavage of the ether bond. A hydride transfer should take place from phenylmethanolate to phenylmethylium, resulting in the formation of benzaldehyde and toluene.

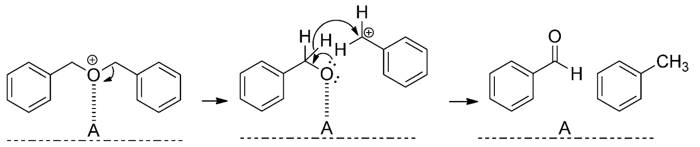

Scheme 1. Proposed reaction pathway for the formation of benzaldehyde and toluene from dibenzyl ether. "A" stands for a Brønsted or Lewis acid site.

Interestingly, the experiments performed with FeS_2 supported on different materials achieved high conversion of dibenzyl ether into arenes (entries 3–8). On the one hand, FeS_2/AC and FeS_2/Al_2O_3 were both highly active and highly selective catalysts, leading to very high to full conversion of dibenzyl ether into toluene (entries 3 and 6). In contrast, FeS_2/SBA-15 and FeS_2/SiO_2 were also highly active catalysts, but less selective to toluene than FeS_2/AC and FeS_2/Al_2O_3. Indeed, in the presence of FeS_2/SBA-15 or FeS_2/SiO_2, the conversion of dibenzyl ether also led to 1,2-diphenylethane, which was formed in carbon yields close to 15 % (entries 4 and 5).

As previously discussed, the supported nanocrystalline FeS_2 phases are air-sensitive. These materials decompose, forming an amorphous material (Figure 3). The experiment performed in the presence of a FeS_2/AC sample exposed to air for 24 h (FeS_2/AC-Air, entry 7) resulted in a 53 % conversion of dibenzyl ether to a mixture comprising toluene (carbon selectivity, 70 %), benzyl alcohol (7 %) and benzaldehyde (23 %). These results compare to those obtained from the experiment with Fe_2O_3/AC (Table 2, entry 8). Nonetheless, there are two features distinguishing FeS_2/AC-Air from Fe_2O_3/AC: 1) the lower carbon selectivity to toluene (70 % with FeS_2/AC-Air vs. 78 % with Fe_2O_3/AC), and 2) the higher carbon selectivity to benzaldehyde (23 % with FeS_2/AC-Air vs. 10 % with Fe_2O_3/AC).

Recyclability of the FeS_2/AC catalyst

Displayed in Table 3 are the results obtained from the experiments of catalyst recycling over three runs, and after the catalyst resulfidation (RSD). The conversion of dibenzyl ether steadily decreased (from 98 to 72 %) throughout the recycling experiments (entries 1–3). In addition, the selectivity to toluene slightly reduced (from 100 to 97 %). After RSD of the spent catalysts with H_2S at 400 °C for 2 h, an 89 % conversion of dibenzyl ether into toluene was achieved. This result shows that the catalytic performance can be partially recovered by RSD.

To assess whether structural changes are occurring in the catalyst on its reuse, the samples of the spent and the resulfided catalyst were analyzed by XRD. Figure 6 shows the XRD patterns, and reveals that the FeS_2 phases were converted into $Fe_{(1-x)}S$ upon the first reaction run. No considerable structural changes could be detected in the XRD pattern of the catalyst samples of the 2nd and 3rd runs. The resulfidation of the spent catalyst could regenerate the FeS_2 phases, but only part of the catalytic performance (Table 3, entry 4).

In the presence of H_2 at temperatures above 200 °C, pyrite is converted into pyrrhotites ($Fe_{(1-x)}S$ where $0 \leq x \leq 0.125$) upon releasing of H_2S.[2,7,8] In the conversion of biomass using metal sulfide catalysts, the addition of a sulfidizing agent to the stream is a common practice in order to keep the high level of catalytic performance.[31,32] Hypothetically, the addition of H_2S could shift the equilibrium towards pyrite. Should FeS_2 (pyrite) or a sulfur-richer member of the

Table 3. Performance of the FeS_2/AC catalyst in the recycling experiments conducted on dibenzyl ether.[a]

Entry	Reaction	Conv. [%]	Carbon selectivity [%]	
			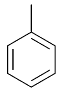	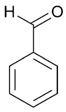
1	1st	98	100	0
2	2nd	84	99	1
3	3rd	72	97	3
4	RSD/4th	89	100	0

[a] Reaction conditions: dibenzyl ether (2.5 mmol), *n*-decane (0.7 mmol, internal standard for GC), FeS_2/AC (0.15 g) and cyclohexane (15 mL, solvent) under 100 bar H_2 (measured at RT), 250 °C for 2 h.

pyrrhotites be the active phase for HDO of dibenzyl ether, the addition of H_2S would be favorable to the reaction performance. Moreover, should H_2S be a homogeneous catalyst for the HDO of dibenzyl ether, the addition of H_2S could also improve the overall reaction performance.

To verify these hypotheses, an experiment with FeS_2/AC under a partial pressure of 1 bar H_2S and 100 bar H_2 was performed. We found that the presence of H_2S has no inhibitory effect on the formation of $Fe_{(1-x)}S$. However, the catalytic results showed a decrease (from 98 to 81 %) in the conversion of dibenzyl ether. Furthermore, the selectivity to toluene dropped (from 100 to 72 %), while the selectivity to benzyl alcohol reached 22 %.

In an attempt to characterize the transformation of the catalyst surface after the HDO of dibenzyl ether, the Fe 2p and S 2p core-level X-ray photoemission (XP) spectra of the 'as prepared' and spent FeS_2/AC (after 1st reaction run) were collected. Figure 7 a shows the Fe 2p XP spectrum of the freshly sulfided catalyst sample. This XP spectrum displays photoemission (PE) peaks typical of FeS_2 compounds with the binding energy peak of Fe $2p_{3/2}$ at 707.1 eV.[22,33,34] Despite the careful handling of the catalyst sample under argon, the low-intensity line at ≈711 eV suggests the presence of a small population of Fe^{II} sites consistent with hydrated iron(II) oxide or iron(II) sulfate.[22,33,34] After the first reaction run, Fe 2p XP spectrum changed significantly. Figure 7 b shows that the narrow signal at 707 eV markedly decreased in intensity. The Fe 2p XP spectrum is dominated by the peak at about 711 eV.

Shown in Figure 7 c is the S 2p XP spectrum for the freshly prepared catalyst FeS_2/AC. The spectrum is a convolution of at least four different sulfur species. The main line at 162.7 eV is characteristic of S_2^{2-} bulk species (pyrite or marcasite, FeS_2). The peak at 161.6 eV is consistent with S^{2-} species that can belong either to bulk sulfides or to S^{2-} surface sites.[22,33,34] The signal at 164.2 eV is assigned to S_8,[22,33,34] suggesting that part of the elemental sulfur content remained in the pore structure of AC. Finally, there is a peak at around 168 eV, which indicates the presence of SO_4^{2-} species associated with Fe^{II} ions.[22,33,34] Again, after the first reaction run, the S 2p XP spectrum also changed considerably. Figure 7 d displays that the signals at 161.4 eV (S^{2-}) and at 163.9 eV (S_8) increased, while S_2^{2-} bulk species (from pyrite or marcasite) decreased in intensity. In ad-

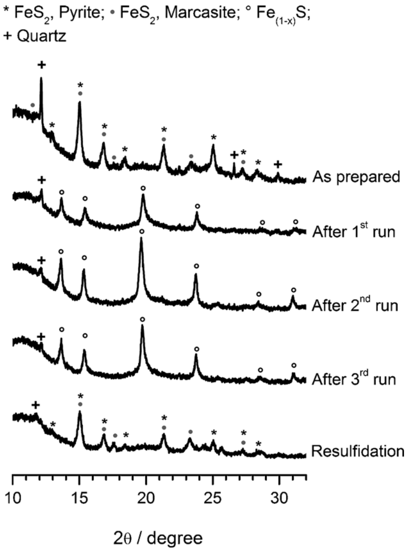

Figure 6. XRD patterns of FeS_2/AC catalyst (as prepared), spent catalysts, and the resulfided catalyst.

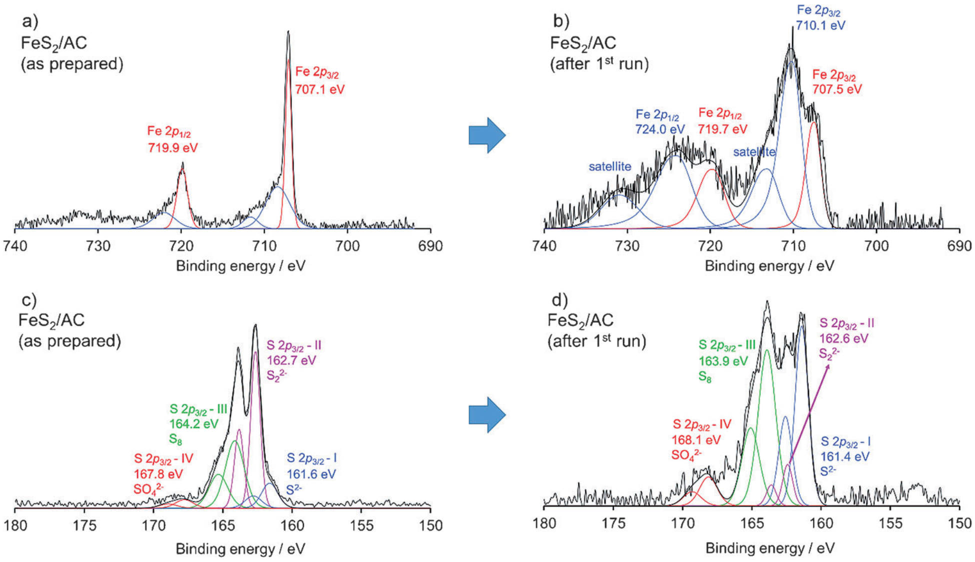

Figure 7. XPS spectrum of the as prepared FeS_2/AC and the used catalyst: a) Fe 2p spectrum of the as prepared catalyst, b) Fe 2p spectrum of the used catalyst, c) S 2p spectrum of the as prepared FeS_2/AC, d) S 2p spectrum of the used catalyst.

dition, the signal for SO_4^{2-} was also more pronounced in the XP spectrum of the spent catalyst than that found for the as-prepared catalyst.

Overall, the current results demonstrate the formation of a fresh surface upon the conversion of FeS_2 into $Fe_{(1-x)}S$ to be the cause of the high activity of pyrite in the HDO of dibenzyl ether to toluene. Unfortunately, XPS results are not very specific. We found that there is a partial desulfurization of the particle surface, which creates a complex chemical environment for Fe- and S-species. Importantly, the addition of H_2S interferes in the formation of the non-stoichiometric pyrrhotite surface responsible for the HDO of dibenzyl ether.

Conclusions

We demonstrated HDO of dibenzyl ether, in the presence of supported nanocrystalline FeS_2 materials, to render high yields of toluene. The recycling experiments showed that the catalyst exhibited relatively good reusability. Throughout the recycling experiments, there is a gradual loss in the conversion of dibenzyl ether and in the selectivity to toluene. However, the spent catalyst could be partially regenerated by resulfidation with H_2S at 400 °C for 2 h. Importantly, XRD and XPS results show that the active phase is not pyrite (FeS_2), but a freshly formed (unknown) surface of $Fe_{(x-1)}S$. Accordingly, there is a clear need for detailed studies on the surface science of iron(II) (di)sulfides and their interaction with hydrogen and with oxygenates. Evident lines of investigations for the future are high-pressure XPS studies and XRD analysis under operando conditions to gain insight into the functionality of the surface structure of the real 'Fe–S' catalyst. Currently, studies are in progress to evaluate the applicability of the pyrite catalyst precursor in the conversion of lignin and lignin-derived phenolics.[35]

Experimental Section

Chemicals

Dibenzyl ether (Aldrich, 99%), *n*-decane (Aldrich, +99%), cyclohexane (Aldrich, +99.9%), SiO_2 (Silica gel, Aldrich, product number 236810) and Al_2O_3 (Aldrich product number 544833) were used as purchased. SBA-15 support was synthesized by a method reported in ref. [36]. Activated carbon (AC) was supplied by NORIT company (Product name: DARCO MRX). To exclude any possible influence of metal impurities on the commercial carbon support, the activated carbon was treated with nitric acid solution (33 wt%) at 80 °C for 24 h, and then washed with deionized water until pH≈7, dried at 120 °C overnight for further use.

Preparation of the supported nanocrystalline FeS_2 catalysts

The supported nanocrystalline FeS_2 catalysts were prepared via incipient wetness impregnation method. The supports (AC, Al_2O_3 SiO_2 or SBA-15) were impregnated with an iron(III) nitrate solution (Table 4), dried at 120 °C for 12 h. In sequence, the material was sulfided with H_2S (50 mL min^{-1}) at 400 °C for 2.5 h. Finally, the sample was cooled down to RT under argon. The supported FeS_2 materials (*air-sensitive*) were stored in closed vials inside a glove box. All procedures involving supported nanocrystalline FeS_2 materials were performed in a glove box under argon.

Table 4. Typical weight information for the synthesis of catalysts with a Fe loading of 10 wt%.

Entry	Support	Weight of support [g]	Weight of $Fe(NO_3)_3 \cdot 9H_2O$ [g]	Volume of Water [mL]
1	AC	1.00	0.72	3.0
2	Al_2O_3	1.00	0.72	0.9
3	SiO_2	1.00	0.72	2.3
4	SBA-15	1.00	0.72	6.5

Characterization methods

Powder X-ray diffraction (XRD) patterns of the samples were obtained by using a STOE STADIP transmission diffractometer operated at 50 kV and 40 mA, using monochromatized Mo-$K_{\alpha 1}$ radiation and a position sensitive detector.

Transmission electron microscopy (TEM) images were taken by using a Hitachi HF-2000 FE transmission electron microscope operating at a voltage of 200 kV. Energy-dispersive X-ray spectroscopy (EDX) analysis was performed by a Noran System Six EDX with a Si (Li) detector.

N_2 sorption experiments were performed by using an ASAP 2000 surface area analyzer (Micromeritics). The specific surface areas of samples were determined using the Brunauer–Emmett–Teller (BET) method. The pore volume and pore size distribution were derived from the desorption profiles of the isotherms using the Barrett–Joyner–Halanda (BJH) method.

X-ray photoelectron spectroscopy (XPS) measurements were performed by using a Kratos HSi spectrometer with a hemispherical analyzer. The monochromatized $Al_{K\alpha}$ X-ray source (1486.6 eV) was operated at 15 kV and 15 mA. For the narrow scans, a pass energy of 40 eV was applied. The hybrid mode was used as lens mode. The base pressure during the experiment in the analysis chamber was 4×10^{-7} Pa. To account for charging effects, all spectra are referred to C_{1s} XP emission at 284.5 eV.

Hydrogenolysis of dibenzyl ether

Dibenzyl ether (2.5 mmol), catalyst (0.15 g) and 15 mL solvent were placed into a batch reactor (36 mL) under argon (glove box). After purging the reactor with H_2, the reaction vessel was loaded with 100 bar H_2 (25 °C). The experiments were performed at 250 °C for 2 h (the reaction time was recorded upon reaching 250 °C (the time required for increasing the temperature from 25 to 250 °C was 30 min) under mechanical stirring (300 rpm). The products were analyzed by GC-MS and GC-FID.
The carbon yield and selectivity was determined as given by Equation (1) and (2), respectively:

$$\text{Yield}(\%) = \frac{n_{\text{product}} \times N_{\text{productcarbon}}}{n_{\text{substrate}} \times N_{\text{substratecarbon}}} \times 100 \quad (1)$$

$$\text{Selectivity}(\%) = \frac{\text{Yield}_{\text{product}}}{\text{Conversion}_{\text{substrate}}} \times 100 \quad (2)$$

where: n_{product} is the amount of product (in mmol) determined by GC-FID, $N_{\text{product carbon}}$ is the number of carbon atoms in a product,

$n_{\text{substrate}}$ is the amount of remaining substrate (mmol), $N_{\text{substrate carbon}}$ is the number of carbon atoms in the substrate.

Acknowledgements

The funds for this research have been provided by the Alexander von Humboldt Foundation in the framework of the Sofja Kovalevskaja Award 2010 endowed by the German Federal Ministry of Education and Research. This work was performed as part of the Cluster of Excellence "Tailor-Made Fuels from Biomass", which is funded by the Excellence Initiative of the German federal and state governments to promote science and research at German universities. The project "Sustainable Chemical Synthesis (SusChemSys)" is co-financed by the European Regional Development Fund (ERDF) and the state of North Rhine-Westphalia, Germany, under the Operational Program "Regional Competitiveness and Employment" 2007–2013.

Keywords: hydrodeoxygenation · iron · lignin · lignite · sulfides

[1] S. Vasireddy, B. Morreale, A. Cugini, C. Song, J. J. Spivey, *Energy Environ. Sci.* **2011**, *4*, 311 – 345.
[2] P. A. Montano, Y. C. Lee, A. Yeyeodu, C. H. Chien, *ACS Symp. Ser.* **1986**, *301*, 416 – 429.
[3] J. Zakzeski, P. C. A. Bruijnincx, A. L. Jongerius, B. M. Weckhuysen, *Chem. Rev.* **2010**, *110*, 3552 – 3599.
[4] U. Schuchardt, O. A. Marangoni Borges, *Catal. Today* **1989**, *5*, 523 – 531.
[5] D. W. Goheen, *Adv. Chem. Ser.* **1966**, *59*, 205 – 225.
[6] P. Fei-Ling, C. Chin-Hua, S. Zakaria, N. Soon-Keong, L. Tze-Khong, *Sains Malays.* **2011**, *40*, 221 – 226.
[7] R. M. Baldwin, S. Vinciguerra, *Fuel* **1983**, *62*, 498 – 501.
[8] S. Yokoyama, R. Yoshida, H. Narita, K. Kodaira, Y. Maekawa, *Fuel* **1986**, *65*, 164 – 170.
[9] D. R. Alfonso, *J. Phys. Chem. C* **2010**, *114*, 8971 – 8980.
[10] J. H. Chen, L. H. Lan, Y. Chen, *Miner. Eng.* **2013**, *46 – 47*, 136 – 143.
[11] G. V. Gibbs, D. F. Cox, K. M. Rosso, N. L. Ross, R. T. Downs, M. A. Spackman, *J. Phys. Chem. B* **2007**, *111*, 1923 – 1931.
[12] K. Ramesha, R. Seshadri, C. Ederer, T. He, M. A. Subramanian, *Phys. Rev. B* **2004**, 70.
[13] R. S. Sun, M. K. Y. Chan, G. Ceder, *Phys. Rev. B* **2011**, 83.
[14] C. H. Zhao, J. H. Chen, B. Z. Wu, X. H. Long, *Trans. Nonferrous Met. Soc. China* **2014**, *24*, 491 – 498.
[15] K. M. Rosso, *Rev. Mineral. Geochem.* **2001**, *42*, 199 – 271.
[16] F. A. Cotton, G. Wilkinson, C. A. Murillo, M. Bochmann in *Advanced inorganic chemistry*, Wiley, New York, **1999**, pp. 507 – 508.
[17] D. J. Vaughan, A. R. Lennie, *Sci. Prog.* **1991**, *75*, 371 – 388.
[18] H. S. Genin, J. A. Ibers in *Transition Metal Sulphides, Vol. 60* (Eds.: T. Weber, R. Prins, R. van Santen), Springer, Netherlands, **1998**, pp. 1 – 35.
[19] H. Wang, *Miner. Process. Extr. Metall. Rev.* **2008**, *29*, 1 – 41.
[20] H. P. Wang, I. Salveson, *Phase Transitions* **2005**, *78*, 547 – 567.
[21] A. I. Vogel, G. Svehla, *Vogel's qualitative inorganic analysis*, Longman, **1996**.
[22] D. Brion, *Appl. Surf. Sci.* **1980**, *5*, 133 – 152.
[23] K. M. Rosso, D. J. Vaughan, *Rev. Mineral. Geochem.* **2006**, *61*, 557 – 607.
[24] S. V. Mikhalovsky, Y. P. Zaitsev, *Carbon* **1997**, *35*, 1367 – 1374.
[25] W. J. Huff, J. C. Holtz, *Ind. Eng. Chem.* **1930**, *22*, 639 – 645.
[26] V. Y. Korobkov, E. N. Grigorieva, O. V. Senko, I. V. Kalechitz, *Fuel Process. Technol.* **1988**, *19*, 243 – 252.
[27] X. Wang, R. Rinaldi, *Energy Environ. Sci.* **2012**, *5*, 8244 – 8260.
[28] X. Wang, R. Rinaldi, *ChemSusChem* **2012**, *5*, 1455 – 1466.
[29] X. Wang, R. Rinaldi, *Angew. Chem. Int. Ed.* **2013**, *52*, 11499 – 11503; *Angew. Chem.* **2013**, *125*, 11713 – 11717.
[30] M. R. Sturgeon, S. Kim, K. Lawrence, R. S. Paton, S. C. Chmely, M. Nimlos, T. D. Foust, G. T. Beckham, *ACS Sustainable Chem. Eng.* **2014**, *2*, 472 – 485.
[31] B. Pawelec, J. L. Garcia Fierro in *Catalytic Hydrogenation for Biomass Valorization* (Ed.: R. Rinaldi), The Royal Society of Chemistry, Cambridge, **2015**, Chapter 8, pp. 174 – 203.
[32] J. Roberto Gomes, S. Bezergianni, J. L. Zotin, E. F. Sousa-Aguiar in *Catalytic Hydrogenation for Biomass Valorization* (Ed.: R. Rinaldi), The Royal Society of Chemistry, Cambridge, **2015**, Chapter 9, pp. 204 – 222.
[33] Y. Cai, Y. Pan, J. Xue, Q. Sun, G. Su, X. Li, *Appl. Surf. Sci.* **2009**, *255*, 8750 – 8760.
[34] K. Laajalehto, I. Kartio, P. Nowak, *Appl. Surf. Sci.* **1994**, *81*, 11 – 15.
[35] P. Ferrini, R. Rinaldi, *Angew. Chem. Int. Ed.* **2014**, *53*, 8634 – 8639; *Angew. Chem.* **2014**, *126*, 8778 – 8783.
[36] D. Zhao, J. Feng, Q. Huo, N. Melosh, G. H. Fredrickson, B. F. Chmelka, G. D. Stucky, *Science* **1998**, *279*, 548 – 552.

Received: January 16, 2015